Fracture in glassy polymers: a molecular modeling perspective

2009 J. Phys.: Condens. Matter 21 463101

(http://iopscience.iop.org/0953-8984/21/46/463101)

IOP Publishing Journal of Physics: Condensed Matter

J. Phys.: Condens. Matter **21** (2009) 463101 (17pp) doi:10.1088/0953-8984/21/46/463101

TOPICAL REVIEW

Fracture in glassy polymers: a molecular modeling perspective

Jörg Rottler

Department of Physics and Astronomy, University of British Columbia, 6224 Agricultural Road, Vancouver, BC, V6T 1Z1, Canada

E-mail: jrottler@phas.ubc.ca

Received 10 August 2009, in final form 14 September 2009
Published 26 October 2009
Online at stacks.iop.org/JPhysCM/21/463101

Abstract

Over the past 25 years, molecular modeling and simulations have provided important insights into the physics of deformation and fracture of glassy polymers. This review presents an overview of key results discussed in the context of experimentally observed polymer behavior. Both atomistic and coarse-grained polymer models have been used in different deformation protocols to study elastic properties, shear yielding, creep, physical aging, strain hardening and crazing. Simulations reproduce most of the macroscopic features of plasticity in polymer glasses such as stress–strain relations and creep response, and reveal information about the underlying atomistic processes. Trends of the shear yield stress with loading conditions, temperature and strain rate, and the atomistic dynamics under load have been systematically explored. Most polymers undergo physical aging, which leads to a history-dependent mechanical response. Simulations of strain hardening and crazing demonstrate the nature of polymer entanglements in the glassy state and the role of local plasticity and provide insight into the origin of fracture toughness of amorphous polymers.

(Some figures in this article are in colour only in the electronic version)

Contents

1. Introduction

Amorphous polymers are being used in countless applications ranging from packaging materials to structural components and adhesives. Polymer glasses exhibit many desirable mechanical properties such as a large elastic limit, high ductility and fracture toughness [1, 2]. Many polymers are good glass formers and readily avoid crystallization upon cooling from melt temperatures. The resulting amorphous structure does not have long-range order, which implies that plastic deformation does not occur through the motion of dislocations, which are the carriers of plasticity in crystalline materials. In addition, the presence of long chain molecules and the resulting topological constraints (entanglements) are responsible for unique phenomena at large strains such as strain hardening and crazing. The combination of amorphicity and chain

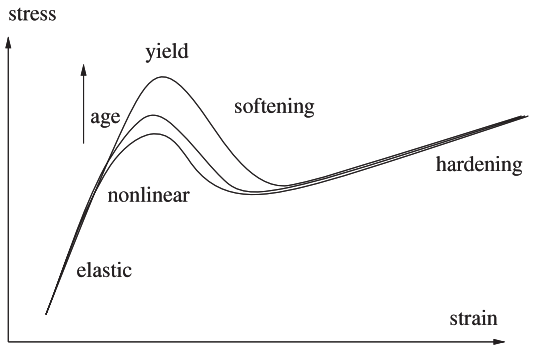

Figure 1. Sketch of a typical stress–strain response of a glassy polymer in uniaxial tension. The yield peak increases with increasing age or waiting time, but the subsequent strain hardening is age-independent.

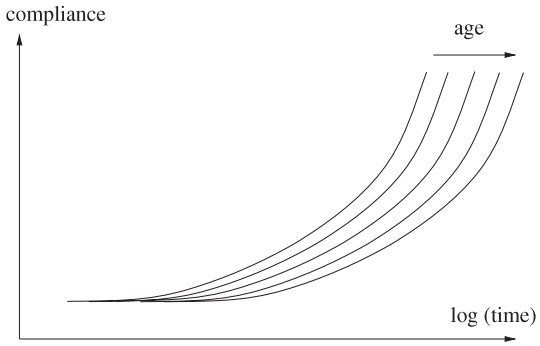

Figure 2. Sketch of typical creep compliance curves of a glassy polymer in the linear regime for several increasing material ages.

connectivity endows polymer glasses with those desirable properties that we make use of every day.

In order to develop models that reliably predict the material lifetime to failure, it is necessary to gain insight into the molecular level processes occurring in amorphous polymers during yield, flow and fracture. From a fundamental perspective, many open questions remain regarding the mechanisms of glass formation, the relaxation processes in the glass and the kinetics during deformation. Molecular simulations are a powerful tool to obtain information about the physics and mechanics of amorphous solids. The mechanical response of small representative volume elements to applied stresses or strains can be obtained simultaneously with detailed information about individual molecular trajectories.

The present review summarizes some key results from computational studies of deformation, yield and fracture in glass-forming polymers on the molecular level that were obtained in the past 25 years. The review will follow the distinct features of the deformation process that can, for instance, be identified on a typical stress–strain curve of a polymer glass. As can be seen in figure 1, an initial linear elastic response is followed by a nonlinear regime that ends in a maximum or overshoot stress, which is often used to define a yield stress σ_y. This yield point is reached for typical strains of 0.05–0.1. Most polymers then exhibit a strain softening regime of negative slope. The subsequent response can have two distinct forms. If void nucleation is avoided, the material undergoes strain hardening and the stress rises again until failure. Alternatively, the polymer develops crazes and the material is converted into a network of fibrils at lower density.

The specific form of the stress–strain curve, and hence the yield stress, is a function of many parameters that include temperature, strain rate, loading conditions and sample history [3]. The dependence on material age is particularly intriguing and a consequence of the nonequilibrium nature of the glassy state. Since the glass has excess volume and entropy over the crystal, it undergoes a slow evolution to its equilibrium configuration during which the properties of the material change. For instance, the yield stress increases with waiting time t_w elapsed since the glass was formed (see figure 1). The aging behavior of the yield stress is particularly important, since it promotes strain localization and hence limits the fracture toughness. In contrast, the behavior at larger strains (hardening and crazing) is age-independent, since the material history has been erased by plastic flow. While less important for the onset of yielding, the parameters of chain length (molecular weight) and entanglement length now control the behavior.

The mechanical response can alternatively be probed by applying a constant load σ and measuring the resulting strain $\epsilon(t, t_w)$ or creep compliance $J(t, t_w)$ [4, 5]. In this experiment, the dependence of the response on two time arguments becomes particularly obvious. As can be seen in figure 2, compliance curves shift to longer times as t_w increases, indicating that the material becomes less compliant with increasing age.

While the first computer simulation studies have focused on elastic behavior and mechanistic aspects of the onset of yielding, more recent work has addressed all aspects of polymer deformation to varying extents. Simulations build a bridge between experimental macroscopic behavior and molecular level insight into the local distributions of atomistic rearrangements and stresses that occur during yield and flow. In this way, new information can be gained that is difficult or impossible to obtain from experiments. Simulations inform continuum models and provide crucial input and tests for the construction of microscopic theories of glassy dynamics. Establishing connections between molecular and macroscopic properties lies at the core of research on the mechanical performance of polymeric systems [6]. By comparing results for different polymers and different levels of molecular modeling, the present review will examine progress as well as open questions. Our focus here will be on molecular level simulations only. It is not our intent to provide a review of the large area of constitutive modeling. Additionally, the discussion will be limited to plasticity and fracture and will not discuss in detail the physics of the glass transition [7].

An overwhelming majority of simulation studies have focused on thermoplastics such as the vinyl polymers polyethylene (PE), polypropylene (PP) and polystyrene (PS) as well as polycarbonate (PC). From a molecular modeling perspective, these hydrocarbon molecules can be studied at two different levels of detail. All force fields are classical; *ab initio* simulations of amorphous polymers are still mostly

out of reach. The first class of models seeks an atomistic representation that captures as much chemical detail as possible. To this end, one may represent explicitly every atom on the polymer chain and compute its interaction with all other atoms. Almost without exception, these short ranged, van der Waals interactions are modeled using the well-known truncated Lennard-Jones (LJ) potential:

$$V_{\mathrm{LJ}}(r) = 4u_0\left[\left(\frac{a}{r}\right)^{12} - \left(\frac{a}{r}\right)^{6}\right] \qquad \text{for } r < r_c, \quad (1)$$

where u_0 and a set the reference energy and length scale. In addition to these pairwise interactions, intrachain interactions such as bond, angle and dihedral (torsional) forces are necessary to accurately describe the stereochemistry of the molecule. The force fields are parameterized by fitting to a combination of *ab initio* data and experimental target functions. A common simplification consists of grouping some atoms such as a CH_2 group into one unit. Such models are referred to as united-atom models and often yield better results than all-atom models. Most atomistic simulation studies of glassy polymers are based on united-atom models, which are easier to treat computationally.

An alternative approach seeks to find simplified, minimalistic models that are not specific to a particular polymer, but instead capture the essential features of chain molecules. Coarse-grained models of the bead–spring type are sufficient to create linear, self-avoiding chains with all generic features of hydrocarbons. A popular metamodel of this type was introduced in 1990 by Kremer and Grest (KG) and consists of repeat units on the carbon backbone interacting via LJ potentials joined together with stiff springs [8]. There are no dihedral interactions, but an angle potential can be added with minimal overhead to change the chain stiffness and hence the Kuhn length l_{K}. Despite its minimalist structure, extensive simulation studies with this model have shown that it describes very well the topological constraints or entanglement that determine the rubbery response of polymer melts [9]. Subsequently, detailed studies of the slowing down of the dynamics due to caging effects in the supercooled liquid regime have been performed [10]. The presence of covalent bonds prevents crystallization and the model undergoes a computer glass transition into a glassy phase that can be used as a starting point for inquiries into mechanical properties.

Both atomistic and coarse-grained models can be studied using either molecular statics (MS) or molecular dynamics (MD) simulations. In MS, the energy of the system is reminimized after incremental strains, while in molecular dynamics Newton's equations of motion are integrated at finite temperature. MD therefore enables the investigation of thermally activated processes and rate-dependent effects. Occasionally, Monte Carlo (MC) dynamics has also been employed. The two levels of modeling have distinct advantages and disadvantages. Atomistic simulations can reveal specific mechanisms of molecular level processes and can be matched quantitatively to experimental data, but are much more limited in size and timescale than coarse-grained models. Contemporary MD simulations can reach up to 100 nanoseconds for tens of thousands of atoms, but the corresponding strain rates and cooling rates are still about 10 orders of magnitude greater than experimental rates. It is also very difficult to equilibrate long, entangled chains in atomistic simulations. Coarse-grained models alleviate some of these limitations, since they gain orders of magnitude in time due to softer potentials (hence allowing a larger timestep), fewer atoms (reducing the number of interaction sites) and faster chain diffusion (due to the removal of explicit side groups) [11]. It is therefore more convenient to use coarse-grained models if generic trends are sought and a wide parameter space is to be investigated. Although many yield and fracture phenomena can readily be observed in both levels of modeling, constructing systematic links between atomistic and coarse-grained models is highly desirable. Such efforts are under way, but have so far focused mostly on polymers in the melt phase [12–14]. Both levels of modeling have produced important insights and therefore complement each other well.

Polymer glasses are certainly not the only kind of amorphous solids. This class of materials includes, for instance, amorphous metals, colloids and many soft glasses such as gels and suspensions. While the processes of strain hardening and crazing require the presence of chain connectivity, the onset of elastoplastic deformation and yield can be expected to have many commonalities across these kinds of materials. In the discussion of yield phenomena, we will therefore also include some studies that have used a coarse-grained model for amorphous metals. This model was introduced by Kob and Andersen in 1995 and consists of a binary mixture of LJ particles of different sizes [15]. Since the onset of plastic deformation is mostly controlled by the nonspecific LJ interaction and not by chain connectivity, it is useful to compare the mechanical response of this model to the polymer, of which it represents the nonbonded limit [16].

The present review is organized according to the main features of a glassy stress–strain curve as displayed in figure 1. Elastic and plastic response will be examined in section 2. Aging effects, which are important for all glassy polymers, will be addressed in section 3. The large-strain phenomena of strain hardening and crazing follow in sections 4 and 5.

2. Elastoplastic behavior and yielding

2.1. Atomistic molecular statics of polypropylene and polycarbonate

Molecular level modeling of polymer glasses began in 1986 with a study by Theodorou and Suter [17, 18]. In their model for atactic polypropylene (a-PP), van der Waals interactions between atoms on different polymers were modeled via an LJ potential, and torsional potentials were employed to describe the energy cost for rotations about the polymer backbone; covalent bond lengths and bond angles were fixed [19]. The authors relaxed the structure via MS and obtained elastic constants from imposing small strains $\epsilon \sim 10^{-3}$ that were in excellent agreement with experimental values [17]. The calculation of the average elastic response was continued with an analysis of the distribution of *local* atomic displacements and atomic stresses [18]. Obtaining such information is a

great advantage of conducting computer simulations, as these quantities are not readily available in experiments. An atomic stress tensor (at zero temperature) at site k may be obtained from the virial stress [20]:

$$\sigma_{ij}^{k} = -\frac{1}{2v_k}\sum_{n\neq k}^{N} r_i^n F_j^n, \tag{2}$$

where F_j^n denotes the j component of the force acting between atoms k and n and r_i^n is the i component of the separation vector. Also needed is a relevant atomic volume v_k, which is often taken as that of a Voronoi cell associated with atom k. For bonded systems with three-body interactions, an additional contribution from the torques must be included [17]. Fluctuations in the atomic stresses are large and their values can be an order of magnitude higher than bulk stresses. Distributions of local shear (deviatoric) stresses are skewed and exhibit a pronounced tail at large stresses; similar results apply to the distribution of nonaffine displacements, which are obtained by subtracting the affine contribution from the bulk deformation tensor from the total particle displacements. The increased likelihood of large rearrangement events and shear stresses is a signature of spatial heterogeneity of amorphous packings and was also observed in simulations of a model metallic glass [21].

The same polymer model and methodology was subsequently used by Mott *et al* for a study of yielding and irreversible plastic deformation at strains up to $\epsilon \sim 0.2$ [22]. The simulations contained between 455 and 3000 atoms, and the computational procedure was equivalent to simulating deformation at zero temperature in the limit of vanishing strain rate. In isotropic materials, it is convenient to describe the stress state in terms of two invariants, the hydrostatic pressure $p = -(\sigma_1 + \sigma_2 + \sigma_3)$ and the deviatoric (von Mises) shear stress:

$$\begin{aligned}\tau_{\text{dev}} &= \tfrac{1}{3}[(\sigma_1-\sigma_2)^2 + (\sigma_2-\sigma_3)^2 + (\sigma_3-\sigma_1)^2]^{1/2} \\ &= \frac{1}{\sqrt{3}}[(\sigma_1+p)^2 + (\sigma_2+p)^2 + (\sigma_3+p)^2]^{1/2},\end{aligned} \tag{3}$$

where σ_i are the principal stress components. Plotting τ_{dev} against the equivalent strain resulting from axial extension and pure shear deformation revealed a gradual transition from elastic behavior at small strains to a plastic flow regime at strains >0.1 with a yield point at strains between 0.05 and 0.07. The stress response is highly intermittent, with discrete stress drops corresponding to localized and irreversible molecular events releasing stress and pervading the entire simulation volume. The deformation is reversible between plastic events, and the first irreversible event occurred already at $\epsilon \sim 0.01$, well within the regime of average linear response. Despite considerable effort, no distinct configurational change or rearrangement related to the chain structure could be identified. By combining measurements of the strain accommodated by a single plastic event with experimental data, an estimate of $\sim$10 nm for the size of a 'shear transformation zone' was given. Such a number appears large and may be due to the fact that the polymer model used fixed bond lengths and bond angles [23].

Many of these features of amorphous plasticity were also found in simulations of a model for polycarbonate developed by Hutnik *et al* [24, 25]. As in the case of PP, the average response is linear up to strains of $\sim$0.06, where plastic yielding sets in. Strain is accommodated by discrete cooperative shear transformation events, and the size of the deforming zones was also estimated to be $\sim$8 nm. The PC system was reported to densify under deformation, in contrast to PP, which exhibited a tendency to dilate. Distinct motions of the various chemical groups (phenylene rings, carbonate and isopropylidene groups) were observed but all contributed equally to the overall deformation. A review of these early computational studies of plasticity in glassy polymers can also be found in [3].

2.2. *Atomistic molecular simulations of polyethylene*

Computer deformation experiments using MD provide important additional information, since they include the effects of finite temperature and give true dynamical trajectories. In 1991, Brown and Clarke studied an amorphous system formed by a single united-atom polyethylene (PE) chain of 1000 monomers at temperatures between 10 and 500 K during uniaxial tension [26]. Polyethylene is the simplest of all vinyl polymers: each CH_2 repeat unit was represented by an LJ bead and linear chains are formed by coupling the beads together with stiff harmonic springs. Additionally, bond angle potentials and dihedral angle potentials were imposed so that the model differentiates between gauche and trans conformations. This study was the first to show that most of the phenomenology of yield and flow of glassy polymers can be captured successfully by such an approach. Despite cooling rates of 1 K ps^{-1}, the increase in density upon cooling from the melt has the qualitative shape of a glass-forming material, with the rate of increase slowing towards lower temperatures. In a subsequent deformation experiment, the simulation box was deformed by increasing a uniaxial stress at a fixed rate of order 1 bar ps^{-1}, and the resulting stresses and strains were recorded. Stress–strain curves averaged over the entire sample show that, as the temperature is decreased, the material supports stresses up to larger and larger strains before yielding (see also [27]). A clear maximum stress develops at strains of $\sim$0.2, which is shown to increase with decreasing temperature and deformation rate. These trends are in good qualitative agreement with experiments, but no quantitative comparisons were attempted.

Slightly reparameterized forms of the PE model were subsequently used by several other researchers. A decade later, Capaldi *et al* published an insightful MD study that was among the first to connect macroscopic material response with observations of enhanced molecular level activity under deformation [28]. In this work, a system composed of 40 000 PE monomers was subjected to uniaxial compression at a constant strain rate. By cooling the material at constant pressure from the melt state, a glass transition temperature of $T_g = 280$ K was reported. This value lies well within the experimental range and depends on chain length and ambient pressure [29, 30]. Figure 3 shows a stress–strain curve of the PE model, which exhibits all qualitative features of that shown in figure 1. The model overestimates the

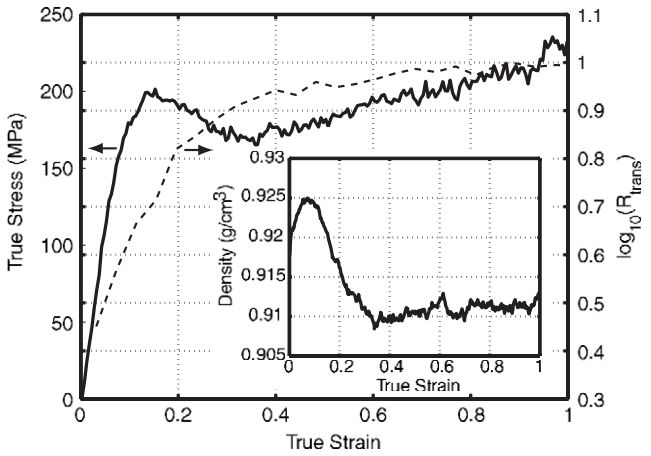

Figure 3. Compressive true stress (solid line) and logarithm of dihedral transition rate R_{trans} (dashed line) versus strain for a PE system at $T = 200$ K deformed at constant strain rate 0.01/ps. Inset: density as a function of strain. Reproduced with permission from [28], ©(2002) by the American Physical Society.

magnitude of the yield stress due to limitations in accessible strain rates and equilibration of the initial structure, but reproduces a well-defined stress overshoot, followed by strain softening and hardening. The salient finding in this study was an accompanying rise in transitions between dihedral trans/gauche states as the deformation progresses. This increase in molecular mobility under deformation is a general theme that has also been investigated through the mean-squared displacement of monomers and the decay of bond-autocorrelation functions (see below). In the PE model, the energy barrier for dihedral flips is significantly lower than that for bond angles and distances, so that molecular rearrangement occurs preferably through this intrachain mechanism. Interestingly, the authors report no change in the bond angle distribution and no spatial correlation between the occurrence of dihedral transitions and local density fluctuations. The increase in molecular mobility is also strongly dependent on strain rate: when deformation is stopped, the dihedral transition rate decays rapidly closely following the macroscopic stress relaxation [28].

Capaldi *et al* also investigated the dependence of the yield stress on strain rate at two different temperatures [31]. Over 2.5 orders of magnitude in strain rate, two regimes of weak and strong logarithmic rate dependence were reported. Logarithmic rate sensitivity is a signature of activated processes and had simultaneously been reported for the coarse-grained KG polymer model [32] (see below). It is often described by Eyring's concept of stress-biased activation over energy barriers [33], which predicts a stress-dependent relaxation time of the form

$$t_{\text{rel}} = t_0 \exp(\Delta E/k_{\text{B}}T) \exp(-\sigma v^*/k_{\text{B}}T). \qquad (4)$$

Here t_0 is a pre-exponential factor, ΔE is a characteristic energy barrier and v^* is called the activation volume. By setting $t_{\text{rel}}^{-1} = \dot{\epsilon}$ when $\sigma = \sigma_{\text{y}}$ one obtains $\sigma_{\text{y}} \propto (k_{\text{B}}T/v^*) \ln(\dot{\epsilon}\tau_0)$. The numerical value of v^* was reported here as 210 Å^3, but a direct molecular level interpretation of this quantity in terms of a physical volume is problematic [34]. If used to estimate the diameter of the implied transformation volume, the resulting value of 2.86 nm is significantly smaller than those reported in [22, 25].

In addition to the molecular dynamics approach, Chui and Boyce [35] and Li *et al* [36] simulated deformation of PE via Monte Carlo (MC) dynamics. In this method, small configurational changes are proposed and accepted with Metropolis rates [37]. Deformation was imposed in small incremental steps and the effect of varying strain rate was mimicked by varying the number of MC updates between strain increments. The resulting dynamics differs in many aspects from true molecular dynamics: the dynamics is diffusive (no inertia) and there is no intrinsic timescale associated with the MC moves. Although the Metropolis algorithm will sample a canonical ensemble and is often used for calculating equilibrium configurations, it is less clear how physically meaningful the resulting trajectories are in a highly nonequilibrium situation. Despite these considerations, the macroscopic stress–strain behavior obtained with the MC method is qualitatively consistent with that found in MD with respect to the shape of the stress response and its dependence on temperature and rate. Additionally, Chui and Boyce considered several different loading conditions and reported an increase of the yield stress with hydrostatic pressure (see also below). These studies also took advantage of the information available in MD simulations and investigated the partitioning of the total stress into inter- and intramolecular contributions. Both intra- and intermolecular interactions rise to a plateau near the yield point, but the interchain stress then drops in the region of strain softening. The study by Li *et al* extended this approach by introducing multiple MC moves that improve equilibration and performs a detailed comparison of elastic moduli, yield stresses and strain hardening moduli.

2.3. Atomistic molecular dynamics of polystyrene and polycarbonate

In a series of papers, Lyulin and collaborators conducted an extensive investigation of the mechanical behavior of atactic polystyrene [38–40] and bisphenol-A polycarbonate [38]. These polymers have a richer chemical structure than PE due to the presence of phenyl side groups (PS) and the difference between carbonate and isopropylene groups and benzene rings (PC). All simulations involve deformation at constant strain rate of order $\sim 10^8$ s^{-1} and explore effects of temperature, pressure and cooling rate on the macroscopic mechanical response as well as certain aspects of molecular rearrangements during the deformation process. Figure 4 shows examples of stress–strain curves for PS and PC. The overall form is again similar to figure 1, but the atomistic force field reveals significant differences between the two polymers. Glass transition temperatures determined from volume versus temperature curves during continuous cooling at 0.05 K/ps imply values of $T_{\text{g}} = 385$ K (PS) and 433 K (PC), which overestimate experimental values only slightly. Reported values for Young's modulus Y of 2.9 GPa (PS) and 2.2 GPa

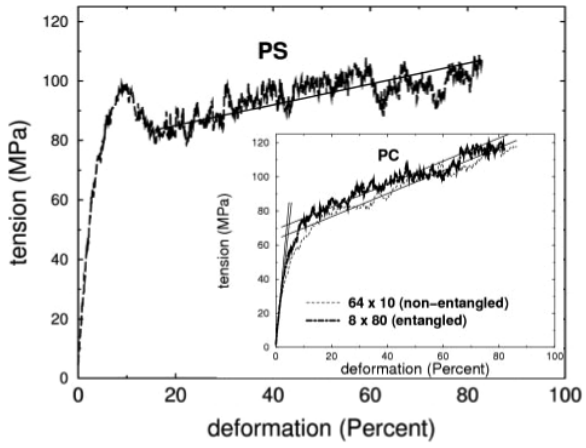

Figure 4. Stress–strain curves from atomistic simulations of uniaxial deformation of PS and PC at $T = 300$ K. The PS system contained 4 chains of 160 monomers, while the PC system contained 64 chains of 10 monomers and 8 chains of 80 monomers, respectively. Reproduced with permission from [38], ©(2005) by EDP Sciences.

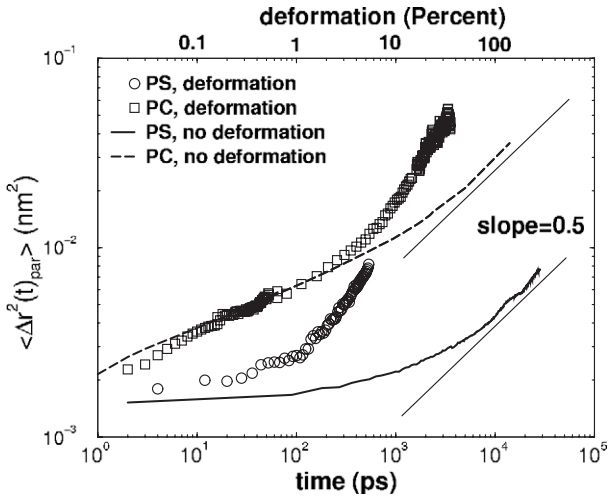

Figure 5. Mean-squared displacement corrected for macroscopic (affine) deformation in the stretching direction in simulations of PS and PC (see figure 4). Reproduced with permission from [38], ©(2005) by EDP Sciences.

(PC) [38] are within 10% of experimental values; yield stresses σ_y of 100 MPa (PS) and 70 MPa (PC) are equally close (within 5%). Such good agreement of key bulk material properties is encouraging yet surprising given the huge difference in cooling and strain rates. It results from the generally weak (logarithmic) rate dependence in polymer glasses.

Reference [39] studied the temperature dependence of Y and σ_y for PS and found a linear variation with T for both quantities in the temperature range of 240–350 K. Fits to an Eyring model gave a value of $v^* = 360$ Å^3. For the same polymer, Vorselaars *et al* [40] studied the pressure dependence of the deviatoric stress at yield under uniaxial deformation for several different normal stresses and reported it to be consistent with the linear relation

$$\tau_{\mathrm{dev}}^{\mathrm{y}} = \tau_0^{\mathrm{y}} + \alpha p, \tag{5}$$

where p is the hydrostatic pressure. This expression is also known as the pressure-modified von Mises yield criterion and predicts a tensile-compressive asymmetry of the yield stress in agreement with the trend seen in the MC simulations for PE. The parameter α may be understood as a friction coefficient. Additionally, $\tau_{\mathrm{dev}}^{\mathrm{y}}$ increases with decreasing cooling rate. All these dependences are not specific to PS, but are general features of glassy polymers and are further discussed in section 2.4 in the context of coarse-grained simulations.

Some specific details of the deformation of PS are, however, revealed upon inspection of detailed atom motion. Reference [39] reported that the planes of the phenyl side groups orient preferably perpendicular to the direction of deformation. A more general finding is again the increase of mobility under deformation. Figure 5 shows the behavior of the mean-squared displacement of backbone monomers in the direction of deformation for the simulations of PS and PC. In this figure, the trivial contribution from the overall affine deformation was subtracted. In both cases, the displacement increases markedly over that of an undeformed sample once the strain exceeds the yield strain. This phenomenon mirrors qualitatively the increase in intrachain torsional transitions described above for PE, although this observable already increased markedly prior to yield.

Another interesting insight from simulations comes from an analysis of the partitioning of the total energy and stress into contributions from the different types of interactions. Reference [40] found that both interchain and intrachain forces contribute to the yield and softening behavior in PS. In the hardening regime, the intrachain contribution to total energy and stress becomes more important. The interchain stresses decrease under extension due to a decrease in density, but remain mostly constant under compression. While the cooling rate only affects the interchain van der Waals component of the energy, both intra- and interchain stress contributions increase upon slower cooling.

2.4. Coarse-grained molecular dynamics

Many of the phenomena found in the atomistic simulations described above are not tied to the chemistry of a particular polymer and can already be seen with coarse-grained models such as the KG polymer. As discussed in section 1, in this model several repeat units on the carbon backbone are represented by LJ spheres coupled together with stiff springs. It is important to realize that, despite its simplicity, the KG model already provides an excellent representation of the simplest polymer, polyethylene, whose atomistic united-atom model differs only by the presence of dihedral terms and a specific mapping of potential parameters. The KG model forms the basis of a large number of simulation studies, whose key results are discussed subsequently.

2.4.1. Yield stress. The study by Vorselaars *et al* [40] reported that the yield stress of PS can be described by a pressure-modified von Mises criterion equation (5). Indeed this condition is most commonly quoted for glassy polymers.

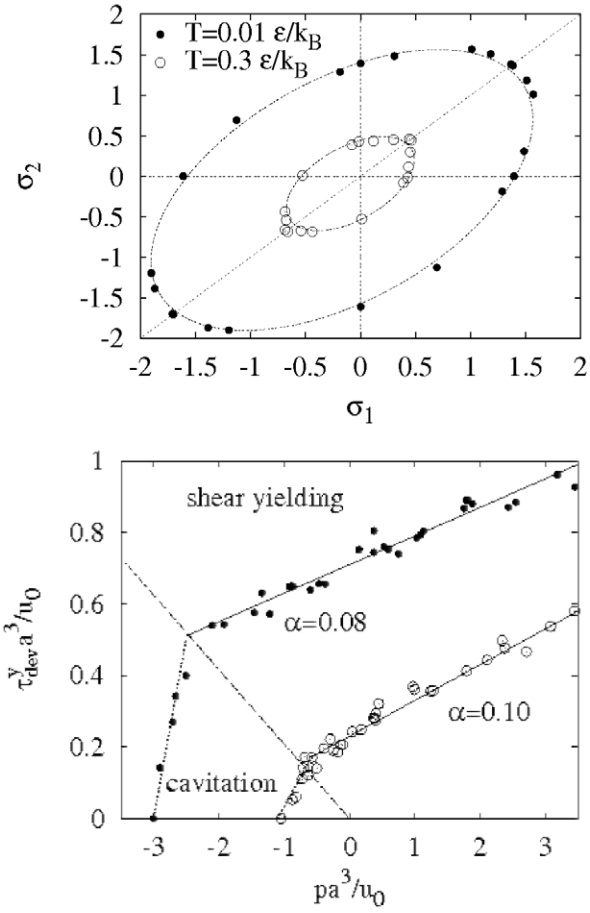

Figure 6. (a) Yield surface of the KG polymer model for two temperatures under biaxial loading conditions. σ_i denote the principal stress components. (b) Deviatoric stress $\tau_{\rm dev}$ (equation (3)) at yield versus pressure. Straight lines are fits to equations (5) and (14). Reprinted from [41], ©(2002) by the American Physical Society.

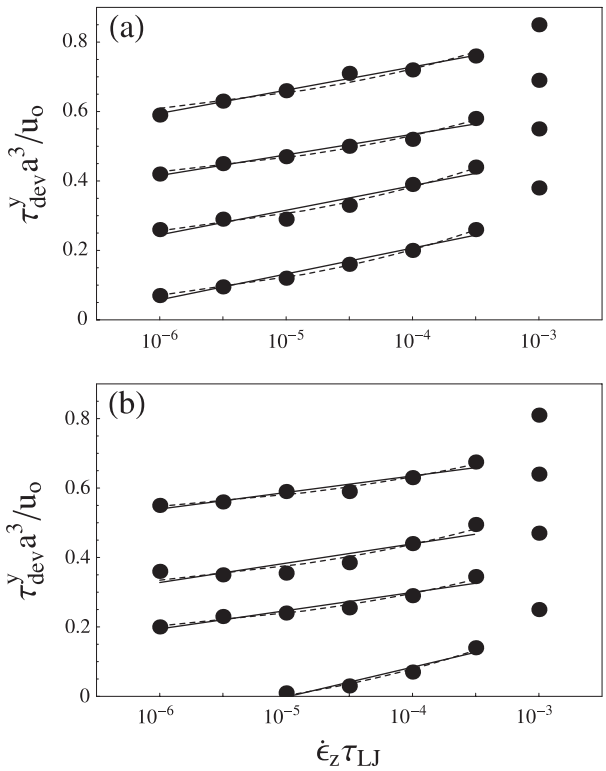

Figure 7. Strain rate dependence of the deviatoric stress at yield for the KG model (a) and the KA binary mixture (b). The temperature decreases from $T = 0.3u_0/k_{\rm B}$ to $0.01u_0/k_{\rm B}$ with intermediate values of $T = 0.2u_0/k_{\rm B}$ and $0.1u_0/k_{\rm B}$. Also shown are fits to a logarithmic (solid) and power law (dashed) rate dependence. Reprinted from [32], ©(2003) by the American Physical Society.

Rottler and Robbins [42] investigated the applicability of this criterion for a wider range of multiaxial loading conditions [42]. The stress–strain curve of the KG model is qualitatively similar to that shown previously for the atomistic models, and also exhibits a yield point at strains between 0.05 and 0.1. Deformation was imposed by deforming a fully periodic simulation box, but simulations with nonperiodic boundary conditions that mimic force clamps yield qualitatively similar results [43]. Figure 6(a) shows the yield surface for strictly biaxial loading conditions. In this case, equation (5) predicts an elliptical yield surface, which is in excellent agreement with results from the KG model at two glassy temperatures and also with the yield behavior of polymethylmethacrylate (PMMA) [44, 45] (for PS forming shear bands, these experiments suggest better agreement with a modified Tresca criterion). The same data presented in figure 6(b) as deviatoric stress versus pressure is also well fitted by equation (5) as long as failure occurs through shear. In coarse-grained simulations, it is customary to report all quantities in reduced simulation (LJ) parameters. In figure 6(b), for instance the unit of stress is therefore u_0/a^3, which would correspond to roughly 50 MPa.

An important result from this study was that, while the magnitude of the offset $\tau_0^{\rm y}$ is strongly dependent on temperature and the adhesive component of the LJ potential (determined by its range), the value of the friction coefficient $\alpha \approx 0.1$ is not. Chain length and rigidity do not strongly affect either quantity, indicating that yield is dominated by short-range intermolecular processes. As the loading condition becomes triaxial, the mode of failure changes from shear yielding to cavitation (see section 5).

Rottler and Robbins also examined the dependence of shear yielding on strain rate and temperature. The flexibility of the KG model permitted a systematic exploration of three decades in strain rate at four temperatures below $T_{\rm g}$. Figure 7(a) summarizes the behavior of the yield stress for a volume-conserving shear deformation. In agreement with the work of Capaldi *et al* on PE [31], a regime of weak rate dependence at lower rates changes into a stronger rate sensitivity at high rates. The behavior at small rates could be described either with a logarithm or a power law. A key observation that can be made in figure 7(a) is, however, that the slope of the logarithmic rate dependence is almost independent of temperature, even though T varies by a factor of 30. This result contradicts the simple Eyring expression equation (4), which predicts a linear temperature dependence. The temperature dependence of the yield stress itself, however, is simpler and as expected: $\tau_{\rm dev}^{\rm y} \propto (T_{\rm g} - T)$ for temperatures $T < T_{\rm g}$.

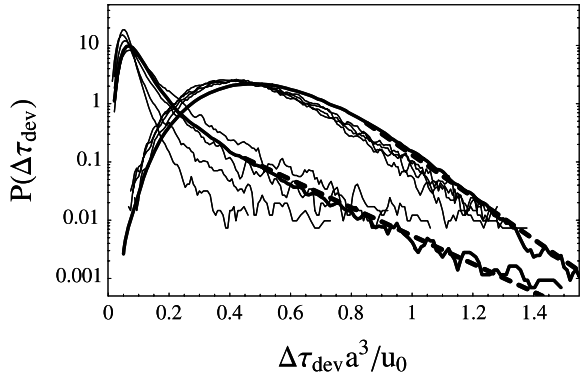

Figure 8. Distribution of stress jumps of amplitude $\Delta\tau_{\rm dev}$ in the KA mixture during deformation at two different temperatures $T = 0.01u_0/k_{\rm B}$ and $0.3u_0/k_{\rm B}$. Different curves belong to increasing strains of 0, 0.025, 0.045 and 0.07 (from left to right), while the thick solid line corresponds to the steadily sheared state. Dashed lines are exponential fits to the tails of the steady state distributions. Reprinted from [32], ©(2003) by the American Physical Society.

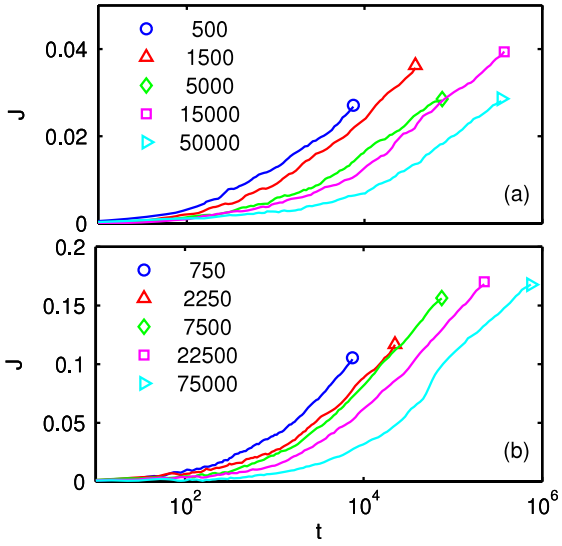

Figure 9. Plastic compliance $J_{\rm pl}(t, t_{\rm w}) = \epsilon(t, t_{\rm w})/\sigma - J_{\rm el}$ of a KG polymer system containing 80 000 beads at a glassy temperature of $T = 0.2u_0/k_{\rm B}$ for various waiting times $t_{\rm w}$ indicated in the legend in units of $\tau_{\rm LJ}$. A uniaxial load of (a) $\sigma = 0.4u_0/a^3$ and (b) $\sigma = 0.5u_0/a^3$ is applied to the aged glasses. Reprinted from [55], ©(2007) by the American Physical Society.

Deviations from simple Eyring type behavior can be explained by the presence of other out-of-equilibrium degrees of freedom that contribute to the activation of plastic events over barriers [46, 47]. Theoretical and computational work on the nature of such an 'effective temperature' in sheared glassy materials [48–52] and its usefulness as an internal state variable is ongoing. An alternative, more microscopic model was introduced by Chen and Schweizer, who replace equation (4) with [53]

$$t_{\rm rel} = t_0 \exp(E/k_{\rm B}T) \exp(a F_{\rm B}(T, \tau)/k_{\rm B}T). \qquad (6)$$

In this theory, the relaxation time is controlled by an effective free energy barrier $F_{\rm B}$, whose temperature dependence is determined by the (temperature-dependent) amplitude of long wavelength density fluctuations. $F_{\rm B}$ also decreases under an applied stress. An advantage of this formulation is that, unlike the Eyring model, stress operates directly on microscopic dynamical variables via distortion of the free energy that controls the segmental relaxation.

Panel (b) of figure 7 presents results for the same quantities and control parameters from simulations of the binary (KA) mixture without covalent bonds. As can be seen, all qualitative features are preserved, indicating again that, in LJ-based glass formers, chain connectivity is not strongly influencing the mechanical response at small strains. For this reason, we briefly discuss measurements of the static yield stress $\sigma_{\rm st}$ of the KA mixture by Varnik and Barrat [54], where simple shear at fixed rate $\dot\gamma$ was imposed by confining the molecular glass between two solid walls. In order to determine the static yield stress, a different loading protocol must be used, in which the stress is slowly ramped up and yield occurs when the system deforms with a threshold velocity or strain rate. This definition is consistent with yield being the smallest stress required to initiate flow. The static yield stress vanishes above $T_{\rm g}$ and rises as the temperature is lowered towards a maximum value at zero temperature. In the KA mixture, the static yield stress is always larger than the steady state shear stress in the limit of vanishing strain rate (dynamic yield stress). The material is therefore susceptible to shear banding when $\sigma(\dot\gamma) < \sigma_{\rm st}$ [54].

To gain further insight into the microscopic nature of events during plastic deformation, Rottler and Robbins investigated local stresses in small volume elements containing of the order of ten beads. Large changes $\Delta\tau_{\rm dev}$ in the local deviatoric stress over times that are short compared to the inverse strain rate may serve as indicators of the occurrence of local plastic events. Even in the absence of shearing, stress jumps occur due to the influence of thermal noise. Figure 8 shows how these distributions evolve during a deformation at constant strain rate. At a high temperature $T = 0.3\,u_0/k_{\rm B}$ the distributions under deformation do not differ strongly from the unsheared solid. At lower temperature $T = 0.01\,u_0/k_{\rm B}$, however, thermal fluctuations are reduced and shear strongly increases the likelihood of large stress release events in the tail of the distributions. As the system settles into a steady state, a well-defined exponential tail develops that describes the continuing yield processes. The large fluctuations reflect the spatially heterogeneous yield events in the glassy material.

2.4.2. Creep compliance. In all simulation studies described so far, a constant strain rate deformation protocol was employed. In experiments, however, it is equally common to apply stress directly to the sample and to measure the resulting strain $\epsilon(t, t_{\rm w})$ as a function of time. As mentioned in the Introduction, the response is, in general, history-dependent and also depends on the waiting time $t_{\rm w}$ elapsed since vitrification. Warren and Rottler [55] and Riggleman *et al* [56, 57] have recently used this protocol to investigate additional features of the deformation of polymer glasses. In such studies it is customary to report the creep compliance $J(t, t_{\rm w}) = \epsilon(t, t_{\rm w})/\sigma$, where σ is the applied stress. A typical response can be seen in figure 9 for two values

of σ in the nonlinear regime and several different waiting times t_w. The creep response shifts to longer times as the waiting time or age of the sample increases, a signature of physical aging discussed further below. Reference [56] reported several important observations. First, a significant variability in the response for small samples that converged for sample dimensions larger than 30 bead diameters was observed (system sizes in figure 9 as well as those in the previous section are all larger than this size), which suggested that the material is mechanically heterogeneous below a characteristic length scale [58]. The authors then investigated the decay of bond-autocorrelation functions $C_b(t) = \langle P_2(\hat{b}(t) \cdot \hat{b}(0))\rangle$ as a measure of local molecular mobility ($\hat{b}$ are unit vectors along the polymer backbone and P_2 is the second Legendre polynomial). By fitting the autocorrelation functions to stretched exponential functions of the KWW form, $C_b(t) = \exp[-(t/\tau)^\beta]$, a characteristic time τ was extracted. This bond angle decorrelation time is related to the average strain rate of the deforming sample in a power law fashion irrespective of tensile or compressive loading; indeed one would expect that $1/\tau \sim \dot{\epsilon}$ when the sample deforms with global rate $\dot{\epsilon}$. The same scaling was confirmed for relaxation times obtained from other measures of the dynamics such as the decay of the incoherent intermediate scattering function:

$$F_s(q, t, t_w = 0) = \frac{1}{N}\left\langle \sum_{i=1}^{N} \exp(i\mathbf{q}\cdot[\mathbf{r}_i(t+t_w) - \mathbf{r}_i(t_w)]) \right\rangle \quad (7)$$

when probed at wavevectors comparable to the interparticle spacing [57]. The simulations describe correctly the large increase in segmental mobility under stress observed in experiments [59], which is also a core ingredient in current theories of nonlinear creep [60, 61].

Interestingly, no correlation between τ and volume of the samples was found, leading the authors to suggest that free volume is not controlling enhanced mobility under load. Instead, [57] suggested that a good correlation exists between the relaxation time and the change in inherent structure energy relative to the undeformed state. The inherent structure energy can be obtained from any molecular configuration by an energy minimization technique. In such a picture, the stress-modified potential energy landscape governs the dynamics through thermally activated motion. MD simulations conducted with a more complicated multistep loading protocol modeled on that used in the experiments were able to track detailed features of deformation-induced changes in molecular mobility with remarkable accuracy [62].

2.4.3. Heterogeneity. A defining characteristic of glassy materials is the presence of dynamical heterogeneity [63]. Recent experimental probes of segmental mobility during deformation of polymer glasses via a photobleaching technique give strong evidence that relaxation times not only decrease by up to two orders of magnitude, but the relaxation time spectrum also narrows considerably [59]. In experiments, the reduction of heterogeneity is inferred from an increase in the KWW exponent β. A simulation study by Wallace and Joos has reported closely related observations: when a polymer glass was subjected to a small instantaneous shear strain, the distribution of particle mobilities narrowed while the glass relaxed from the deformation [64].

3. Physical aging

Despite the fact that almost all polymer glasses age, the underlying causes and mechanisms of aging are among the least understood aspects of polymer dynamics. Due to the nonequilibrium nature of the glassy state, polymer properties are not stationary, but slowly evolve in time even in the absence of deformation. A general observation is that bulk thermodynamic variables such as volume and enthalpy decrease logarithmically with the waiting time t_w elapsed since the glass was formed [4, 5]. Yield stress and creep compliance are also history-dependent, which can be used to probe the evolution of structural relaxation times.

3.1. Influence of aging on mechanical properties

The pioneering work by Struik [4] showed that the age-dependent compliance (see figure 2) of many polymers obeys a time–waiting time superposition principle: compliance curves superpose by rescaling time with a waiting-time-dependent shift factor $a_J(t_w) \sim t_w^{-\mu}$. The double logarithmic shift factor $\mu = -\mathrm{d}\log(a)/\mathrm{d}\log(t_w)$ is referred to as the aging exponent. The power law increase of the shift factor only holds true at intermediate times; both for ultrashort times and for very long times (when the glass equilibrates) the aging dynamics ceases and $\mu = 0$ [65]. The power law increase of relaxation times can be obtained in trap models [66] and also in the more microscopic theory of Chen and Schweizer via relaxation kinetics of the amplitude of density fluctuations [67, 68]. In simulations of LJ glass formers, physical aging can readily be observed through two-time correlation functions such as the intermediate scattering function $F_s(q, t, t_w)$ (equation (7)), which obeys a similar scaling behavior [69]. Warren and Rottler demonstrated that the plastic part of the creep compliance obtained from the bead–spring polymer model (figure 9) also follows a superposition principle [55, 70]. In addition to the bulk mechanical response, they monitored simultaneously $F_s(q, t, t_w)$ and the mean-squared displacement $\langle \Delta r^2\rangle = \langle(\mathbf{r}_i(t + t_w) - \mathbf{r}_i(t_w))^2\rangle$. Results for the latter quantity are shown in figure 10 and illustrate the typical behavior of glassy systems: a short ballistic regime is followed by a plateau where particles only move in local cages from which they finally escape diffusively. Cage escape times become longer with increasing age, reflecting the increasing structural relaxation times. The mean-squared displacement curves also obey a superposition principle, and the shift factors a_{msd} obtained from these curves closely track a_J from the mechanical measurement. Microscopic particle mobility is therefore directly related to mechanical response.

As illustrated in figure 1, physical aging also tends to increase the yield or overshoot stress σ_y. Utz *et al* [71] studied stress–strain curves of the KA model using an energy minimization technique and found an increase of the overshoot

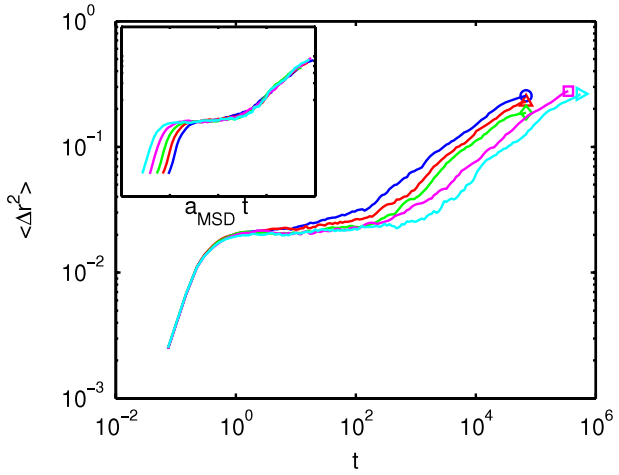

Figure 10. Aging effects in the mean-squared displacement of polymer segments for waiting times t_w as in figure 9. The inset shows that the data can be superposed by shifting time with a shift factor a_{msd}. Reprinted from [55], ©(2007) by the American Physical Society.

stress with decreasing cooling rate, followed by an erasure of the sample history once the sample is undergoing plastic flow. In simulations by Rottler and Robbins, the behavior of σ_y was explored further for a wide range of temperature, strain rate and age [72]. In general, σ_y increases logarithmically with age, which was also reported by Varnik *et al* [54]. The combined dependence on strain rate and temperature is, however, more complicated. Two regimes of weak and strong logarithmic rate dependence were found, and the crossover occurred when the time to strain to yield was approximately equal to the waiting time. To rationalize this behavior, a rate state model was developed that subsumed the effect of aging in a state variable that acts as an effective waiting time. In particular, the model includes any modifications to the aging behavior during the straining period. The yield stress can be written as

$$\sigma_y = \sigma_0 + s_0 \ln[t_w/t_0 + t_{eff}/t_0] + s_1 \ln[\dot{\epsilon} t_0], \qquad (8)$$

where $t_{eff} \propto \dot{\epsilon}^{-1}$. s_0 and s_1 are phenomenological coefficients that describe the logarithmic sensitivity to age and rate. An approach very similar in spirit was developed independently by Klompen *et al* [73] in the context of experiments on PC.

3.2. Rejuvenation and overaging

The intrinsic aging dynamics of glasses can be altered by mechanical perturbations such as stress or strain. Depending on the deformation protocol, situations can arise in which the material appears younger (rejuvenated) or older (overaged) compared to an unstrained sample. The notion of erasure of aging and a resulting stress-induced rejuvenation rests on the observation that the aging exponents μ are found to decrease with increasing probe stress (applied after the polymer was aged under no load) [4, 5]. This effect can be seen in a broad range of glassy polymers. The stressed material therefore appears to have aged less, as if it had been moved back in time closer towards a freshly prepared glass. Simulations by Warren and Rottler [55] reproduce this effect and find the same stress dependence of the mechanical shift factors and those obtained from correlation functions or mean square displacement curves for stresses well into the nonlinear regime. The correct interpretation of these observations, however, remains an intensely debated topic. Although the aging exponent is reduced under applied stress and the volume increases upon loading, the time to reach an equilibrium state and the ensuing volume relaxation is unchanged [65]. Simulated creep curves, when interrupted by a stress pulse, also rapidly return to the original aging trajectory.

An alternative approach to strain-induced rejuvenation and overaging can be taken from an energy landscape perspective. Several studies offer strong evidence that deformation relocates the glass on the potential energy surface. Lacks and Osborne specifically employ a zero-temperature strain cycle and show that, depending on preparation of the quenched glass and maximum strain amplitude, the energy of the system can be increased (rejuvenated) or decreased (overaged) relative to an undeformed sample [74]. Strain release seems to be necessary to observe overaging; shear alone always leads to an increase of the inherent structure energy [75, 76]. Warren and Rottler analyzed the soft glassy rheology (SGR) model [46], which is a trap model augmented by the effect of applied stress and found a transition from overaging to rejuvenation as the (noise) temperature for activated transitions is increased [77]. Experiments on colloidal glasses also support the picture of a repopulation of the energy landscape due to shear, such that long relaxation times are, for instance, overpopulated in the case of overaging [78]. Isner and Lacks concluded that strain does not literally rejuvenate the system, but produces a configuration with a close resemblance to a younger state (shorter relaxation times, etc) [79]. Similar findings were reported by Lyulin and Michels, who simulated strain cycle experiments on atomistic models of PS and PC [80]. In their work, overaging appeared for rapidly quenched samples, while slowly annealed polymers displayed rejuvenation. The authors suggested that rejuvenation (overaging) occurs when the cooling time is much longer (shorter) than the time it takes to strain to yield. However, the energy partitioning between intra- and interchain degrees of freedom was distinct from that of a thermal quench.

Nontrivial changes to the aging trajectory of glasses can also be brought about by thermal histories other than the simple down-quench used in most studies. Montes *et al* found that, if aging in PMMA is interrupted by a temperature step, simple time–aging time superposition no longer holds and regimes of apparent rejuvenation and overaging appear [81]. Simulations modeled on the same experimental temperature protocol revealed the same changes to the relaxation time spectrum [82].

From the above discussion it is clear that several robust features of mechanically induced changes to the aging kinetics are also present in molecular simulations. Aging phenomena are indeed a defining property of glassy materials. Aging occurs not only in polymer glasses, but also in many soft glasses such as colloids [78] and physical gels [83]. It is important to note, however, that the terms ‘rejuvenation’ and

'overaging' are used to describe the effect of different loading protocols (constant stress, strain cycle) on different quantities (compliance, potential energy). More work is needed to bring these different manifestations onto common ground.

4. Strain hardening

The ability of glassy polymers to avoid catastrophic failure after yielding, but instead to continue to deform at increasing stress, forms the basis of many engineering applications. Early simulations by McKechnie *et al* [84] gave strong evidence for a correlation between the large scale conformational structure of polymers and their strain hardening behavior. The atomistic simulations of Capaldi *et al* [28] for PE (see figure 3) and Lyulin *et al* [38, 39] for PS and PC (see figure 4) readily reproduce strain hardening. For uniaxial deformation, stress–strain curves in the hardening regime can be well fitted to a Gaussian (neo-Hookean) form:

$$\pm\sigma = \sigma_0 \pm G_r g(\lambda), \tag{9}$$

where σ is the stress in the deformation direction, $\lambda = L/L_0$ is the stretch and $g(\lambda) = \lambda^2 - 1/\lambda$. The sign in equation (9) depends on whether the deformation is tensile or compressive. G_r is referred to as the hardening modulus. Equation (9) may be generalized to Langevin hardening in highly entangled polymer chains:

$$\pm\,\sigma = \sigma_0 \pm G_r g(\lambda) L^{-1}(h)/3h. \tag{10}$$

Here $L(x)$ is the Langevin function and $h = (\lambda^2 + 2/\lambda)C_\infty/3N_e$ depends on the stiffness constant $C_\infty = l_k/l_0$ as well on the number of beads between entanglements N_e. Reported values of $G_r = 13 \pm 3$ MPa for PS in a temperature range $T = 260$–480 K [39] and $G_r = 12 \pm 0.5$ MPa at $T = 300$ K as well as a higher modulus for PC, $G_r = 22 \pm 1$ MPa [38], are very close to experimental values. For the strain rates and configurations studied, no dependence of strain hardening on entanglements was found. In close similarity to the shear yield stress, the hardening is also pressure-dependent and was found to be well described by the linear relation

$$G_r(p) = G_{r,0} + \mu p, \tag{11}$$

where p is the pressure at yield [40]. Additionally, the ratio of hardening modulus to yield stress remained constant over the range of pressures studied.

Despite the success of the Gaussian model in describing experimental and simulation data, there are serious difficulties and inconsistencies with its theoretical motivation. The functional form arises from an entropic network model and reflects the entropic free energy penalty from stretching the network. While such arguments are well justified for rubbery polymer melts, it is not clear how polymer chains in the glassy state can sample configurations sufficiently fast for entropy to contribute significantly to the overall stress. The hardening modulus is predicted to vary linearly with temperature and entanglement density ρ_e and $G_r = \rho_e k_B T$. Experiments, however, provide strong evidence that G_r instead decreases linearly with increasing T and is about 100 times larger than $\rho_e k_B T$ [85].

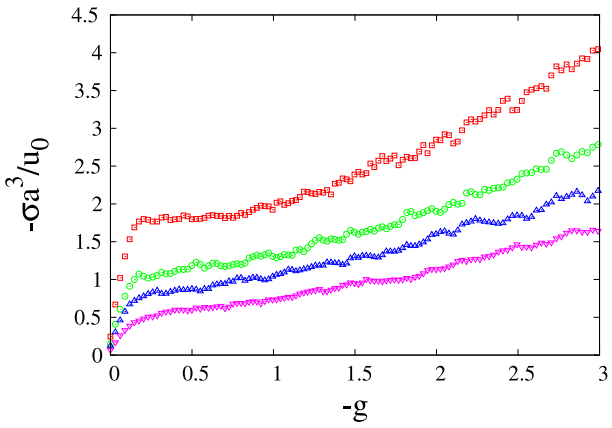

Figure 11. Strain hardening in the KG model with fully entangled, semiflexible chains for compressive uniaxial deformation at four different temperatures $T = 0, 0.1, 0.2$ and $0.3\,u_0/k_B$ from top to bottom. The simulation box contained 70 000 monomers and was deformed at constant true strain rate $\dot{\epsilon}_z = 10^{-4}\tau_{LJ}^{-1}$. Figure courtesy of R S Hoy.

A series of papers by Hoy and Robbins [86–88] resolved these discrepancies and provided an improved interpretation of the molecular origin of strain hardening. All of their simulations are based on the coarse-grained KG model in order to be able to study a wide range of parameters. Since entanglement effects are important for the hardening response, extra care must be taken to create glassy configurations with the correct chain statistics. Equilibration times for long chains can be decreased either with hybrid MD-MC methods that alter the chain connectivity [89] or growth schemes inspired by radical polymerization [90]. Typical hardening curves from simulations are shown in figure 11. The yield stress is independent of entanglement length but increases with decreasing temperature. Subsequently, the stress strongly rises with increasing strain. The functional behavior of the hardening regime crosses over from equations (9) to (10) as the entanglement length decreases, and the modulus obtained from fits to these expressions is indeed proportional to ρ_e (for undiluted polymers) [86].

Figure 11 also displays one of the central results of Hoy and Robbins' work: strain hardening decreases with increasing temperature and the ratio $G_r/\rho_e k_B T$ is reported to vary between 85 and 3800. The simulations reveal the fundamental inconsistency between entropic network models and observed trends of G_r. Instead, the authors made the remarkable observation that the ratio of G_r/σ_{flow} varies relatively little with temperature, where σ_{flow} is the flow stress measured at the onset of strain hardening, $g(\lambda) = 0.5$. The flow stress therefore sets the scale of the hardening modulus. An excellent data collapse was achieved by normalizing the stress–strain curves for varying rates with the flow stress; similar results were obtained for varying the range of adhesive interaction between polymer chains [86]. The authors therefore suggested that, for a fixed temperature, the stress–strain curve obeys a

scaling relation:

$$\sigma(\lambda, \dot{\epsilon}) = F(\lambda)\sigma_{\text{flow}}(\dot{\epsilon}), \tag{12}$$

where $F(\lambda)$ is a scaling function. Subsequent work including a larger range of rates showed, however, that the scaling function $F(\lambda)$ still has a residual dependence on strain rate [91]. Additionally, the ratio G_r/σ_{flow} is not strictly constant but obeys (in simulations [91] and experiments [92]) a linear relation:

$$G_r = C_0 + C_1\sigma_{\text{flow}}. \tag{13}$$

A second important insight from these simulations is that strain hardening occurs also for chains shorter than the entanglement length. Simulations with chain lengths increasing from 4 to 350 beads showed that the hardening modulus increases continuously and saturates once $N \gg N_e$ (figure 12(a)). Hardening is correlated with any measure of large scale chain reorientation. As an example, the authors showed that the mean end-to-end distance R_e of the polymer chains increases in a manner that closely tracks the hardening regime of the stress–strain curves, and reaches a purely affine limit for highly entangled chains (figure 12(b)). Remarkably, stress–strain curves for different chain lengths could be collapsed in figure 12(c) onto a master curve by replacing λ with an effective stretch $\lambda_{\text{eff}} = R_z/R_z^0$ (for a stretch in the z direction; R_z^0 is the undeformed rms end-to-end distance) [87]. This illustrates that the subaffine chain deformation for $N \leqslant N_e$ is correctly captured by R_e.

As a measure of the amount of plastic deformation occurring in the sample, the mean-squared nonaffine segmental displacements were tracked during strain hardening [86]. An intriguingly simple proportionality emerged between this quantity and the entanglement density, suggesting that strain hardening is fundamentally due to an increase in plastic deformation with strain and ρ_e. Further evidence for a connection between local plastic activity and strain hardening came from a decomposition of the total stress $\sigma = \sigma_U + \sigma_Q$ into energetic ($\sigma_U = \partial U/\partial\epsilon$) and thermal ($\sigma_Q = \partial Q/\partial\epsilon$) contributions [87]. While σ_Q has the functional form of the entropic network model, σ_U is very small and only contributes to the total stress at very large strains in the Langevin hardening regime. Hoy and Robbins monitored the rate of plasticity by counting the fraction of nonspecific LJ bonds whose length changed by more than 20% in a strain interval of 0.005. Interestingly, this rate of plastic deformation is perfectly correlated with the thermal stress component σ_Q, including fluctuations. Further evidence for the importance of dissipative processes comes from recent atomistic simulations of glassy PS and PC by Vorselaars *et al*, which found a rise in the rate of nonaffine monomer displacements in the strain hardening regime [93]. The rate sensitivity is higher for PC than PS, suggesting a robust connection to the difference in strain hardening modulus of the two polymers. The fundamental origin of the proportionality between σ_Q and $g(\lambda)$, however, remains unclear. Hoy and Robbins suggested that g indirectly reflects the role of entropy [88]. As the number of conformations available to chains decreases with increasing g, a higher rate of plastic events is needed to accommodate the deformation.

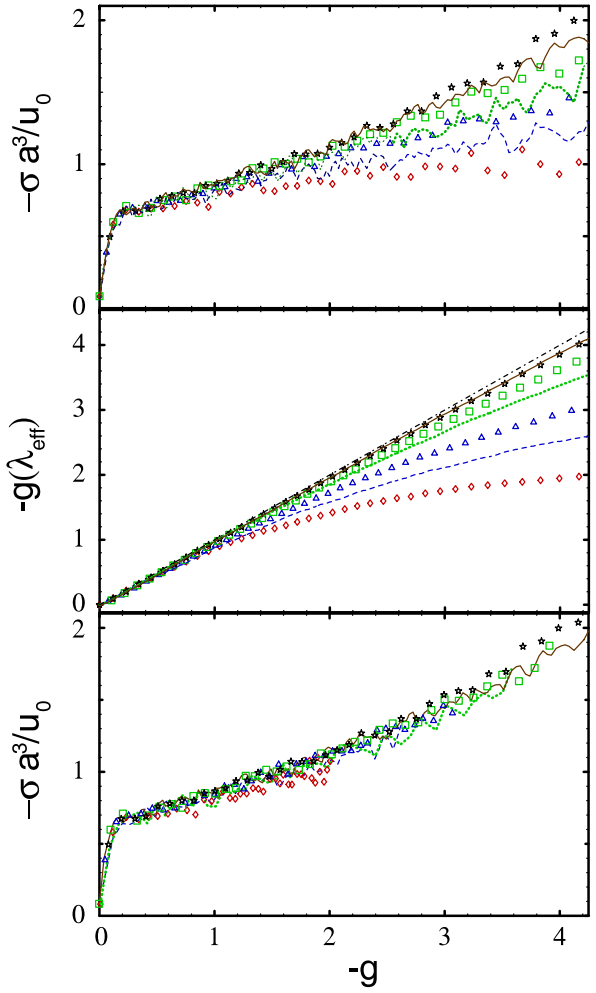

Figure 12. (a) Stress versus $g(\lambda)$ during uniaxial compression at $T = 0.2u_0/k_B$ with true strain rate $\dot{\epsilon}_z = 10^{-5}\tau_{LJ}^{-1}$. Successive curves from bottom to top are for chains of length $N = 10$ (◇), 16 (dashed line), 25 (△), 40 (dotted line), 70 (squares), 175 (solid line) and 350 (stars). (b) $g(\lambda_{\text{eff}})$ versus $g(\lambda)$ for the same systems. (c) Stresses of panel (a) plotted against $g(\lambda_{\text{eff}})$. Reprinted from [87], ©(2007) by the American Physical Society.

5. Crazing

The fracture mechanism of crazing is perhaps one of the most remarkable features of glassy polymers [94–96]. Crazing refers to the conversion of dense polymer into a load-bearing network of fibrils and voids at lower densities. It is frequently observed in PS and PMMA, but less so in tougher polymer such as PC that fail predominantly through shear [2]. As depicted in the inset of figure 13, crazing occurs in the process zone in front of an advancing crack tip. The craze is a deformed region that grows in width d and length l under an applied stress S. Typical values for d and l for glassy polymers are indicated, and the drawing stress S ranges between 20 and 100 MPa. The density ρ_{ini} of the polymer drops to a final value ρ_{fin} by a constant extension ratio $\lambda_{\text{cr}} \equiv \rho_{\text{ini}}/\rho_{\text{fin}}$; typically $\lambda_{\text{cr}} = 2$–6. Using the KG model, Rottler and Robbins explored all stages of craze fracture in a series of simulations [41, 97, 98]. Even with a coarse-grained model, however, it is not possible

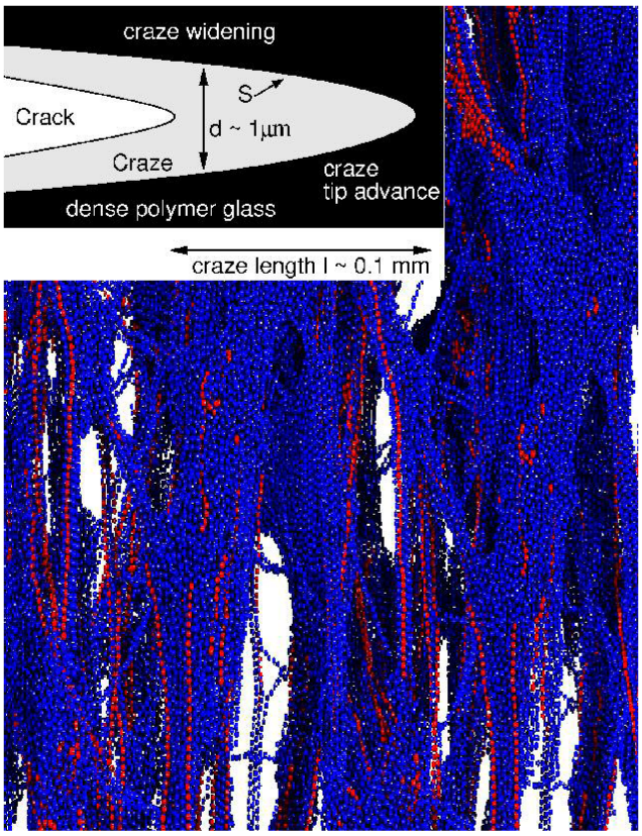

Figure 13. Snapshot of a simulated craze network consisting of fibrils and voids. The simulation box contains 255 000 monomers. Chains that carry the top 10% of the total tension are colored in red (light gray). Inset shows the geometry of craze fracture, reprinted from [41], ©(2003) by the American Physical Society.

to simulate μm^3-sized regions that would include an entire crack tip. Instead, they simulated small representative volume elements representative of craze initiation, craze growth and craze breakdown.

5.1. Craze initiation

Crazing requires the nucleation of microvoids that continue to evolve into the fibril network. In experiments, this happens frequently near defects that generate large local tensile stresses. A transition from shear yielding to cavitation was also observed in the simulations. In figure 6(a) the mode of failure changes as the loading state approaches a purely triaxial tensile load. In the regime where cavitation was observed, the deviatoric shear stress no longer obeys the pressure-modified von Mises criterion. Instead the data was consistent with a cavitation criterion of the form

$$\tau^{\mathrm{c}}_{\mathrm{dev}} = \tau^{\mathrm{c}}_0 + \alpha^{\mathrm{c}} p, \tag{14}$$

where the superscript c indicates cavitation. Other cavitation criteria proposed in the literature [2] are, however, also consistent with the narrow range of pressures under which cavitation occurs.

5.2. Craze growth

Rottler and Robbins simulated craze growth by increasing the size of the periodic simulation box in one Cartesian direction at constant velocity. Once initial cavities are formed, entanglements start to play a crucial role. Chains shorter than twice the entanglement length do not form stable crazes and the stress rapidly drops to zero [99]. For longer chains, however, growth of the cavities is arrested and undeformed polymer is converted into the craze within an advancing active zone. Craze growth continues until all material in the simulation box is drawn into the craze. Figure 13 shows a close-up image of the resulting structure. It can be seen that individual polymer strands have aligned to form fibrils that are aligned with the widening direction. The fibrils frequently merge to form cross-ties.

The extension ratio λ_{cr} is dependent on the entanglement length N_{e}. Experimental values of λ_{cr} are well described by the simple scaling relation [94]

$$\lambda_{\mathrm{cr}} = \lambda_{\mathrm{max}} = \left(\frac{N_{\mathrm{e}} l_0}{l_{\mathrm{p}}}\right)^{1/2}, \tag{15}$$

where l_0 and l_{p} denote the elementary step length and persistence length of the polymer, resp. This expression arises from the supposition that, in the glass, entanglements act like permanent chemical crosslinks. In this case, the initial separation between entanglement points on a random walk polymer, $d_{\mathrm{i}} = (l_{\mathrm{p}} l_0 N_{\mathrm{e}})^{1/2}$, cannot be increased beyond the final length of a straight segment, $l_{\mathrm{f}} = N_{\mathrm{e}} l_0$. The maximum possible extension is therefore $\lambda_{\mathrm{max}} = d_{\mathrm{f}}/d_{\mathrm{i}}$. Simulations confirm equation (15) for several values of N_{e}, but reveal that the argument used to justify it is not entirely correct [41]. By directly analyzing the configurations of chains in the craze structure, Rottler and Robbins showed that the typical length of straight segments that are aligned with the widening direction is not $l_0 N_{\mathrm{e}}$, but rather $l_0 N_{\mathrm{e}}/3$. Segmental displacements indicate that the polymer deforms affinely on large scales, but is pulled taut only over the same short length scale. This result is consistent with the observation $\lambda_{\mathrm{cr}} = \lambda_{\mathrm{max}}$ only if the initial length d_{i} is shorter by a factor $1/\sqrt{3}$. This is, however, the case, since the polymer chains form a random network and only the projected component of d_{i} onto the z axis is expanded. In a regular mesh, all strands would be expanded equally.

The stress σ_{zz} in the straining z direction is shown in figure 14 for chains of different lengths N and two degrees of flexibility as a function of stretch L_z/L. Semiflexible chains have a larger persistence length and shorter entanglement length than flexible chains. The stress–strain curve can be decomposed into three regimes: after an initial peak due to cavitational yielding (regime I), σ_{zz} drops to a plateau or drawing stress S and remains essentially constant (regime II) until crazing is complete and further extension strains the craze network itself until it breaks (regime III). The constant drawing stress S is a characteristic feature of crazing independent of N, but larger for the semiflexible (more entangled) polymers. Similar to the shear yield stress, S decreases linearly with increasing temperature and logarithmically with decreasing strain rate.

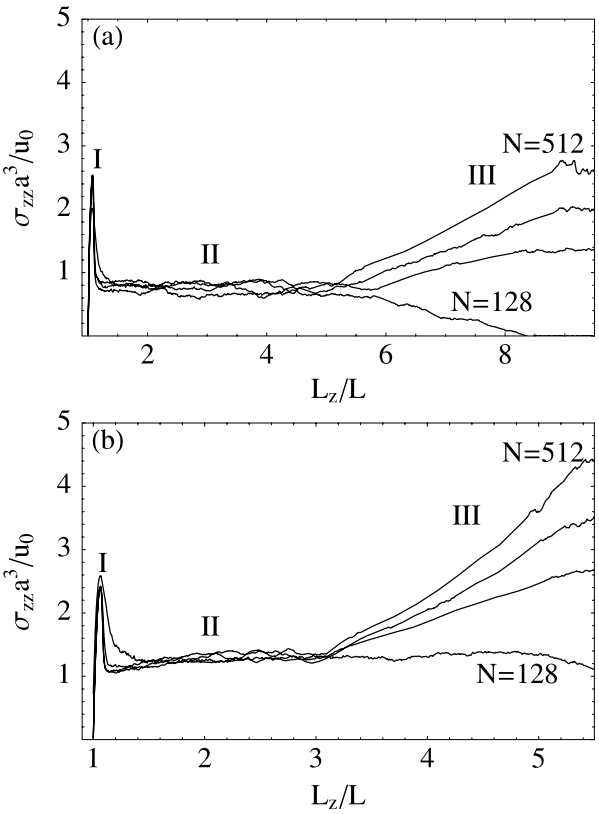

Figure 14. Stress–strain curves of polymer crazing for (a) flexible and (b) semiflexible chains of length $N = 128$, 256, 384 and 512. Three regimes of nucleation (I), growth (II) and failure (III) are indicated (see text). Reprinted from [41] ©(2003) by the American Physical Society.

In traditional models of craze growth, the drawing stress is assumed to arise from capillary effects. The polymer is treated as a viscous fluid, and craze growth occurs through the propagation of void fingers into the strain-softened active zone. The applied stress S then results from dissipative (viscous) contributions as well as a contribution from surface tension. Simulations allow a test of the assumptions behind this model and, similar to the case of strain hardening, reveal inconsistencies. Partitioning the stress into covalent and van der Waals contributions shows that, in the craze, most of the stress is carried by the covalent bonds and only a very small fraction is attributable to surface tension. The covalent contribution is not present in the capillary model. The simulations instead suggest a simpler relation between microstructure and drawing stress of the form $S\lambda = S_0$. S_0 is the local stress within the fibrils that depends on temperature, rate and adhesive interactions. Indeed, stress–strain curves for four different entanglement lengths could be collapsed when the drawing stress is multiplied by λ. S_0 exhibits similar trends with temperature and adhesive interactions than shear yield stress and cavitation pressure. This suggests that the craze drawing stress is closely related to bulk yield properties, as local plastic deformation is needed to rearrange strands into fibrils.

5.3. Craze breakdown and fracture toughness

According to figure 14, straining the craze beyond the extension ratio requires an increase in stress beyond the plateau stress. The stress will continue to rise until the craze fails either through chain pullout or chain scission. In order to explore the crossover between the two failure mechanisms, a phenomenological bond potential was employed in the simulations that leads to chain scission when the force in a covalent bond is 100 times larger than the maximum van der Waals force. Figure 14 shows that the maximum stress $S_{\max}$ required to break the craze is indeed strongly dependent on chain length and rises above the plateau stress only for chains longer than $2N_e$. More generally, the crossover between pullout and scission occurs for $5 < N/N_e < 10$ and $S_{\max}$ saturates for longer chains. Such a transition in failure mode was also seen in the simulations of Sides *et al* [100], who examined the failure of glassy polymers tethered to a substrate using an almost identical polymer model. Adhesive failure either through chain pullout or scission was found to occur at low grafting densities, while for higher grafting densities and longer chains, failure occurred cohesively through bulk crazing.

An important insight was gained by studying the distribution of tension in the polymer chains upon stretching the craze. In a homogeneous material, all bonds carry the same tension and break when the tension exceeds the threshold for bond breaking. Rottler and Robbins found instead that the tensile part of the tension distribution in crazes has an exponential form that becomes wider as the strain increases (see figure 15) [98]. This broad distribution increases the likelihood of large tensions that exceed the breaking threshold. The exponential shape is universal and does not depend on entanglement length or other control parameters. In the breakdown regime, the only parameter required is the average tension $\langle f \rangle$ and distributions normalized by $\langle f \rangle$ collapse onto the same curve. Since exponential tails are frequently observed in the stress distributions of a broad class of amorphous materials under compression, it was suggested that crazes may be viewed as a material that has jammed under tension [41]. Indeed, it is the frictional forces between chains that prevent them from sliding past each other.

Despite the large stress fluctuations, crazes are surprisingly tough. The fracture energy G_c of PMMA or PS is thousands of times larger than the minimum energy $G_{eq} = 2\gamma$ that is required to separate two surfaces with surface tension γ. Calculating G_c is difficult since it involves physics on multiple length scales. G_c is given by

$$\frac{G_c}{G_{eq}} = \frac{SD_0}{2\gamma}\frac{d}{D_0}(1 - 1/\lambda_{cr}), \tag{16}$$

where D_0 is the typical spacing between fibrils. All parameters in this expression can be calculated from molecular simulations with the exception of the craze width d, which is of the order of microns. The maximum width of a craze can, however, be estimated with a linear fracture mechanics model developed by Brown [96, 101], which uses the well-known analytical form

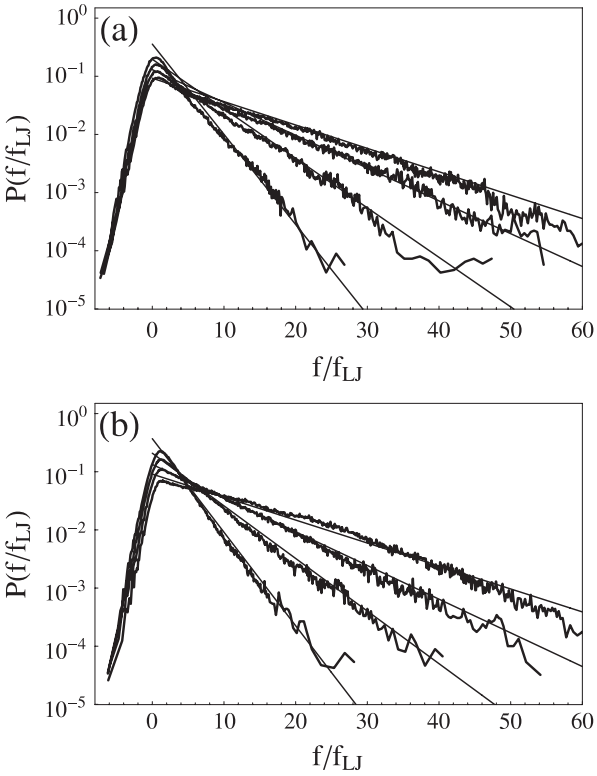

Figure 15. Distribution of tension in polymer crazes for (a) flexible and (b) semiflexible chains. The straight line is a fit of the tails to the exponential form $\exp[-f/\langle f\rangle]/\langle f\rangle$. The four curves correspond to increasing strains in regime III indicated in figure 14. Reprinted from [41], ©(2003) by the American Physical Society.

of the stress singularity in front of a crack tip (see figure 13) to predict

$$\frac{d}{D_0} = 4\pi\kappa\left(\frac{S_{\max}}{S}\right). \tag{17}$$

In this expression $S_{\max}$ is the stress required to break a craze fibril and κ is a function of the anisotropic elastic constants of the craze. In [97], Rottler and Robbins computed both quantities from molecular simulations of crazing, and by combining with the fracture mechanics model, succeeded in predicting the enhancement of fracture energy that is observed in many polymer glasses.

6. Conclusions and outlook

Molecular simulations of glassy polymers capture most of the experimental behavior and reveal detailed information about the mechanisms that are operative during yielding, hardening and crazing. Coarse-grained simulations using the KG or similar bead–spring models appear to be sufficient to analyze general trends with temperature, chain length, entanglement density, deformation rate and material history, but may not capture every detail of the molecular rearrangements during plastic flow in real glasses. The weak logarithmic rate dependence of yielding in the glassy state alleviates the timescale gap between simulations and experiments, so that atomistic simulations make remarkably realistic predictions of elastic moduli Y, yield stresses σ_y and hardening moduli G_r. The dimensionless ratio $\sigma_y/Y = 0.05$–0.1 lies in the typical range of amorphous polymers. The dependence of σ_y on pressure, strain rate, and age can be observed in both atomistic and over a wider range of parameters in coarse-grained models. Both intrachain and interchain dynamics is accelerated under load. Simulations of hardening and crazing have revealed the nature of entanglements in the glassy state, the role of local plasticity and the difficulties with extending models based on entropic elasticity or equilibrium capillary effects into the glassy state.

An area still in need of improved understanding is the kinetics of yielding and the role of thermodynamic temperature. There is now unequivocal theoretical [53], computational [32] and experimental [59] evidence that the simple Eyring model of flow via stress-biased thermal activation over barriers neither accurately describes the relaxation dynamics as a function of true stress [59] nor provides a consistent description over all temperatures. A logarithmic rate dependence of the yield stress is generally found within a limited range of strain rates only, and the dependence of the prefactor on temperature is more complicated. Contemporary theories of plastic deformation in glassy solids emphasize the role of a noise [46] or effective temperature [48–52] in increasing the likelihood of localized plastic events [47, 102], and much of this development has been driven by numerical tests of the proposed measures. Although basic features of the aging kinetics are understood, much uncertainty remains in interpreting the effects of more complicated thermal or mechanical histories that lead to apparent rejuvenation or overaging. Simulations also hold the key to further insight into the fundamental nature of shear transformation zones [103–105] that collectively lead to the macroscopic mechanical response. A recent study, for instance, found that failure occurred preferentially at sites exhibiting small local elastic moduli [106]. It will also be fruitful to compare the polymer response to mechanisms of plasticity in noncovalently bonded amorphous packings [107–109], which can be expected to share many similarities.

A majority of simulation studies have focused on the simplest case of linear, non-crosslinked homopolymers. Highly crosslinked polymer networks form the basis of many adhesives, but have received much less attention. An exception is the work by Stevens *et al* [110–113], which investigated the failure of model networks that were formed similarly to chemically cured epoxies: short bead–spring chains are connected via functionalized crosslinkers and then bonded to solid walls. By studying both random and ordered networks, it was shown that the failure strain is directly controlled by the average minimal path connecting the two walls [110]. Once the polymer bonds are stretched further, the stress begins to rise and the bond will fail either adhesively at the interface or cohesively through chain scission. The location of failure is dependent on the interfacial bond density and, for adhesive failure, both failure strain and stress are proportional to the bond density [111]. Subsequent work explored the effect of mixed crosslinker functionality and found that only the

average functionality controls the mechanical properties of the system [112, 113]. Using a similar approach, Mukherji and Abrams suggested that the strain hardening regime in randomly crosslinked networks is attributable to the formation of microvoids [114, 115].

Simulations are also just beginning to address the huge and technologically important class of polymer nanocomposites (PNC). Studying these materials requires larger system sizes to obtain statistically meaningful averages and are therefore more demanding. Coarse-grained simulations representing nanoparticles as smooth spherical inclusions find that the toughness increases by several times over that of a neat polymer in the rubbery state, but changes much less in the glassy state [116]. The toughness increase was therefore attributed to filler mobility, which is larger in rubbery polymers. Simulations with short nanotube fillers seem to corroborate this result, as they report a measurable toughness enhancement only for high filler concentrations and strongly adhesive polymer–filler interactions [117]. In PNCs, a glassy layer with modified local elastic properties develops near the polymer–nanoparticle interface [118]. The locally modified material properties cause changes of the bulk mechanical performance [119], for instance a stiffening of the polymer and a suppression of the creep response [120]. A recent study focused on physical aging in PNC found large changes in the physical aging rate only in the interfacial polymer layer [121]. Both stiffening or softening of the polymer response were observed depending on the type of polymer–nanoparticle interactions (attractive or repulsive). Since many of these effects are strongly dependent on the specifics of the interface, atomistic simulations in combination with systematic coarse-graining methods can be expected to play a more important role in the future.

Acknowledgments

We thank R S Hoy, A V Lyulin and G C Rutledge for granting permission to reproduce selected figures from their work in this paper, as well as R S Hoy and M D Ediger for a critical reading of this manuscript and helpful comments. We acknowledge the Natural Sciences and Engineering Research Council of Canada for financial support.

References

[1] Ward I M and Sweeney J 2004 *An Introduction to the Mechanical Properties of Solid Polymers* (New York: Wiley)
[2] Haward R N and Young R J 1997 *The Physics of Glassy Polymers* (London: Chapman and Hall)
[3] Stachursky Z H 1997 *Prog. Polym. Sci.* **22** 407
[4] Struik L C E 1978 *Physical Aging in Amorphous Polymers and Other Materials* (Amsterdam: Elsevier)
[5] Hutchinson J M 1995 *Prog. Polym. Sci.* **20** 703
[6] Meijer H E H and Govaert L E 2005 *Prog. Polym. Sci.* **30** 915
[7] Debenedetti P G and Stillinger F H 2001 *Nature* **410** 259
[8] Kremer K and Grest G S 1990 *J. Chem. Phys.* **92** 5057
[9] Everaers R, Sukumaran S K, Grest G S, Svaneborg C, Sivasubramanian A and Kremer K 2004 *Science* **303** 823
[10] Bennemann C, Paul W, Binder K and Duenweg B 1998 *Phys. Rev.* E **57** 843
[11] Nielsen S O, Lopez C F, Srinivas G and Klein M L 2004 *J. Phys.: Condens. Matter* **16** R481
[12] Milano G and Mueller-Plathe F 2005 *J. Phys. Chem.* B **109** 18609
[13] Sun Q and Faller R 2005 *Comput. Chem. Eng.* **29** 2380
[14] Praprotnik M, Site L D and Kremer K 2008 *Annu. Rev. Phys. Chem.* **59** 545
[15] Kob W and Andersen H C 1995 *Phys. Rev.* E **51** 4626
[16] Lorenz C D and Stevens M J 2003 *Phys. Rev.* E **68** 021802
[17] Theodorou D N and Suter U W 1986 *Macromolecules* **19** 139
[18] Theodorou D N and Suter U W 1986 *Macromolecules* **19** 379
[19] Theodorou D N and Suter U W 1985 *Macromolecules* **18** 1467
[20] Irving J H and Kirkwood J G 1950 *J. Chem. Phys.* **18** 817
[21] Srolovitz D, Vitek V and Egami T 1983 *Acta Metall.* **31** 335
[22] Mott P H, Argon A S and Suter U W 1993 *Phil. Mag.* A **67** 931
[23] Argon A S, Mott P H and Suter U W 1992 *Phys. Status Solidi* b **172** 193
[24] Hutnik M, Argon A S and Suter U W 1991 *Macromolecules* **24** 5956
[25] Hutnik M, Argon A S and Suter U W 1993 *Macromolecules* **26** 1097
[26] Brown D and Clarke J H L 1991 *Macromolecules* **24** 2075
[27] Yang L, Srolovitz D J and Yee A F 1997 *J. Chem. Phys.* **107** 4396
[28] Capaldi F M, Boyce M C and Rutledge G C 2002 *Phys. Rev. Lett.* **89** 175505
[29] Yang L, Srolovitz D J and Yee A F 1999 *J. Chem. Phys.* **110** 7058
[30] Negi A and Basu S 2006 *Modelling Simul. Mater. Sci. Eng.* **14** 563
[31] Capaldi F M, Boyce M C and Rutledge G C 2004 *Polymer* **45** 1391
[32] Rottler J and Robbins M O 2003 *Phys. Rev.* E **68** 011507
[33] Eyring H 1936 *J. Chem. Phys.* **4** 283
[34] Argon A S 1993 *Mater. Sci. Technol.* **6** 462
[35] Chui C and Boyce M C 1999 *Macromolecules* **32** 3795
[36] Li J, Mulder T, Vorselaars B, Lyulin A V and Michels M A J 2006 *Macromolecules* **39** 7774
[37] Landau D P and Binder K 2000 *A Guide to Monte Carlo Simulations in Statistical Physics* (Cambridge: Cambridge University Press)
[38] Lyulin A V, Vorselaars B, Mazo M A, Balabaev N K and Michels M A J 2005 *Europhys. Lett.* **71** 618
[39] Lyulin A V, Balabaev N K, Mazo M A and Michels M A J 2004 *Macromolecules* **37** 8785
[40] Vorselaars B, Lyulin A V and Michels M A J 2009 *J. Chem. Phys.* **130** 074905
[41] Rottler J and Robbins M O 2003 *Phys. Rev.* E **68** 011801
[42] Rottler J and Robbins M O 2001 *Phys. Rev.* E **64** 051801
[43] Makke A, Perez M, Lame O and Barrat J-L 2009 *J. Chem. Phys.* **131** 014904
[44] Bowden P B and Jukes J A 1972 *J.Mater. Sci.* **7** 52
[45] Quinson R, Perez J, Rink M and Pavan A 1997 *J. Mater. Sci.* **32** 1371
[46] Sollich P, Lequeux F, Hebraud P and Cates M E 1997 *Phys. Rev. Lett.* **78** 2020
[47] Langer J S 2008 *Phys. Rev.* E **77** 021502
[48] Cugliandolo L, Kurchan J and Peliti L 1997 *Phys. Rev.* E **55** 3898
[49] Ono I K, O'Hern C S, Durian D J, Langer S A, Liu A J and Nagel S R 2002 *Phys. Rev. Lett.* **89** 095703
[50] Berthier L and Barrat J-L 2002 *Phys. Rev. Lett.* **89** 095702
[51] Ilg P and Barrat J-L 2007 *Europhys. Lett.* **79** 26001
[52] Haxton T and Liu A J 2007 *Phys. Rev. Lett.* **99** 195701
[53] Chen K and Schweizer K S 2007 *Europhys. Lett.* **79** 26006
[54] Varnik F, Bocquet L and Barrat J-L 2004 *J. Chem. Phys.* **120** 2788

[55] Warren M and Rottler J 2007 *Phys. Rev.* E **76** 031802
[56] Riggleman R A, Lee H-N, Ediger M D and de Pablo J J 2007 *Phys. Rev. Lett.* **99** 215501
[57] Riggleman R A, Schweizer K S and de Pablo J J 2008 *Macromolecules* **41** 4969
[58] Yoshimoto K, Jain T S, Workum K V, Nealey P F and de Pablo J J 2004 *Phys. Rev. Lett.* **93** 175501
[59] Lee H-N, Paeng K, Swallen S F and Ediger M D 2009 *Science* **323** 231
[60] Chen K, Schweizer K S, Stamm R, Lee E and Caruthers J 2008 *J. Chem. Phys.* **129** 184904
[61] Chen K and Schweizer K S 2008 *Macromolecules* **41** 5908
[62] Lee H-N, Riggleman R A, de Pablo J J and Ediger M D 2009 *Macromolecules* **42** 4328
[63] Ediger M D 2000 *Annu. Rev. Phys. Chem.* **51** 99
[64] Wallace M L and Joos B 2008 *J. Phys.: Condens. Matter* **20** 244130
[65] McKenna G B 2003 *J. Phys.: Condens. Matter* **15** S737
[66] Monthus C and Bouchaud J P 1996 *J. Phys. A: Math. Gen.* **29** 3847
[67] Chen K and Schweizer K S 2007 *Phys. Rev. Lett.* **98** 167802
[68] Chen K and Schweizer K S 2008 *Phys. Rev.* E **78** 031802
[69] Kob W and Barrat J-L 1997 *Phys. Rev. Lett.* **78** 4581
[70] Rottler J and Warren M 2008 *Eur. Phys. J. Spec. Top.* **161** 55
[71] Utz M, Debenedetti P G and Stillinger F H 2000 *Phys. Rev. Lett.* **84** 1471
[72] Rottler J and Robbins M O 2005 *Phys. Rev. Lett.* **95** 225504
[73] Klompen E T J, Engels T A P, Govaert L E and Meijer H E H 2005 *Macromolecules* **38** 6997
[74] Lacks D J and Osborne M J 2004 *Phys. Rev. Lett.* **93** 255501
[75] Wallace M L and Joos B 2006 *Phys. Rev. Lett.* **96** 025501
[76] Wallace M L and Joos B 2006 *Phys. Rev. Lett.* **97** 019904
[77] Warren M and Rottler J 2008 *Phys. Rev.* E **78** 041502
[78] Viasnoff V and Lequeux F 2002 *Phys. Rev. Lett.* **89** 065701
[79] Isner B A and Lacks D J 2006 *Phys. Rev. Lett.* **96** 025506
[80] Lyulin A V and Michels M A J 2007 *Phys. Rev. Lett.* **99** 085504
[81] Montes H, Viasnoff V, Jurine S and Lequeux F 2006 *J. Stat. Mech.* P03003
[82] Warren M and Rottler J 2008 *J. Phys.: Condens. Matter* **20** 244131
[83] Cloitre M, Borrega M and Leibler L 2000 *Phys. Rev. Lett.* **85** 4819
[84] McKechnie J I, Haward R N, Brown D and Clarke J H L 1993 *Macromolecules* **26** 198
[85] van Melick H G H, Govaert L E and Meijer H E H 2003 *Polymer* **44** 3579
[86] Hoy R S and Robbins M O 2006 *J. Polym. Sci.* B **44** 3487
[87] Hoy R S and Robbins M O 2007 *Phys. Rev. Lett.* **99** 117801
[88] Hoy R S and Robbins M O 2008 *Phys. Rev.* E **77** 031801
[89] Auhl R, Everaers R, Grest G S and Plimpton K K S J 2003 *J. Chem. Phys.* **119** 12718
[90] Perez M, Lame O, Leonforte F and Barrat J-L 2008 *J. Chem. Phys.* **128** 234904
[91] Hoy R S and Robbins M O 2009 *J. Polym. Sci.* B **47** 1406
[92] Govaert L E, Engels T A P, Wendlandt M, Tervoort T and Suter U W 2008 *J. Polym. Sci.* B **46** 2475
[93] Vorselaars B, Lyulin A V and Michels M A J 2009 *Macromolecules* **42** 5829
[94] Kramer E J 1983 *Adv. Polym. Sci.* **52/53** 1
[95] Kramer E J and Berger L L 1990 *Adv. Polym. Sci.* **91/92** 1
[96] Creton C, Kramer E J, Brown H R and Hui C-Y 2001 *Adv. Polym. Sci.* **156** 55
[97] Rottler J and Robbins M O 2002 *Phys. Rev. Lett.* **89** 195501
[98] Rottler J and Robbins M O 2002 *Phys. Rev. Lett.* **89** 148304
[99] Baljon A R C and Robbins M O 2001 *Macromolecules* **34** 4200
[100] Sides S W, Grest G S, Stevens M J and Plimpton S J 2004 *J. Polym. Sci.* B **42** 199
[101] Brown H R 1991 *Macromolecules* **24** 2752
[102] Langer J S and Manning M L 2007 *Phys. Rev.* E **76** 056107
[103] Spaepen F 1977 *Acta Metall.* **25** 407
[104] Argon A 1979 *Acta Metall.* **27** 47
[105] Falk M L and Langer J S 1998 *Phys. Rev.* E **57** 1971
[106] Papakonstantopoulos G J, Riggleman R A, Barrat J-L and de Pablo J J 2008 *Phys. Rev.* E **77** 041502
[107] Wittmer J, Tanguy A, Barrat J-L and Lewis L 2002 *Europhys. Lett.* **57** 423
[108] Leonforte F, Bossiere R, Tanguy A, Wittmer J and Barrat J-L 2005 *Phys. Rev.* B **72** 224206
[109] Tanguy A, Leonforte F and Barrat J-L 2006 *Eur. Phys. J.* E **20** 688
[110] Stevens M J 2001 *Macromolecules* **34** 1411
[111] Stevens M J 2001 *Macromolecules* **34** 2710
[112] Tsige M and Stevens M J 2004 *Macromolecules* **37** 630
[113] Tsige M, Lorenz C D and Stevens M J 2004 *Macromolecules* **37** 8466
[114] Mukherji D and Abrams C F 2008 *Phys. Rev.* E **78** 050801(R)
[115] Mukherji D and Abrams C F 2009 *Phys. Rev.* E **79** 061802
[116] Gersappe D 2002 *Phys. Rev. Lett.* **89** 058301
[117] Richardson D G and Abrams C F 2007 *Mol. Simul.* **33** 421
[118] Papakonstantopoulos G J, Yoshimoto K, Doxastakis M, Nealey P F and de Pablo J J 2005 *Phys. Rev.* E **72** 031801
[119] Papakonstantopoulos G J, Doxastakis M, Nealey P F, Barrat J-L and de Pablo J J 2007 *Phys. Rev.* E **75** 031803
[120] Riggleman R A, Toepperwein G N, Papakonstantopoulos G J and de Pablo J J 2009 *Macromolecules* **42** 3632
[121] Liu A Y-H and Rottler J 2009 *J. Polym. Sci.* B **47** 1789